EFFECTS OF NOISE ON LAMB-MODE ACOUSTIC-EMISSION ARRIVAL TIMES DETERMINED BY WAVELET TRANSFORM[#∞]

M. A. HAMSTAD[1,2] and A. O'GALLAGHER[1]
[1] National Institute of Standards and Technology, Materials Reliability Division (853) 325 Broadway, Boulder, CO 80305-3328 USA. [2] University of Denver, School of Engineering and Computer Science, Department of Engineering, Denver, CO 80208, USA.

Abstract

Precise acoustic emission (AE) signal arrival times of the fundamental Lamb modes can be obtained from the arrival time of the peak wavelet transform (WT) magnitude at a particular frequency of interest. Since these arrival times are not determined from a fixed threshold, they are not affected by dispersion, attenuation and source amplitude. They also correspond to a single group velocity and lead to source location results more accurate than those obtained by traditional AE location calculations based on threshold-based arrival times. In this research, noise-free finite-element modeled (FEM) AE signals were combined with experimental wideband electronic noise to form noisy signals. Since the noise-free signal was available, the changes in the WT-based arrival times from noise-free to noise-altered signals could be quantitatively evaluated. Several signal-to-noise (S/N) ratios were examined in a statistical fashion for three important types of AE sources at three propagation distances and at different radiation angles. The arrival times determined by WTs were obtained for the two different frequency-mode combinations (A_0 at 60 kHz and S_0 at 522 kHz) that represent the most energetic portions of the signals in a large 4.7 mm thick aluminum plate. From the arrival times, statistical calculations of linear source location were also studied to evaluate errors in location accuracy caused by noise. Even at S/N ratios as low as 1 to 1, the location error was 2 % or less for a large majority of the cases. The errors in arrival time were also examined using two alternative time-frequency analysis approaches to obtain the arrival times. One algorithm (Choi-Williams) provided significantly improved results for the noisy signals.

Keywords: Acoustic emission modeling, Finite element modeling, Source location, Wavelet transform, Wideband acoustic emission.

1. Introduction

Previous publications [1, 2] have demonstrated the use of wavelet transform (WT) results to extract accurate acoustic emission (AE) signal arrival times in plate structures. This technique determines arrival times that are independent of threshold, source amplitude, attenuation based on geometric spreading, radiation direction and signal dispersion based on propagation distance. Further, the arrival times correspond to a single group velocity (Lamb waves) of an energetic mode-frequency combination in the signal. A wideband AE signal database for several buried-dipole-type sources in a thin aluminum plate was used for these demonstrations. This database was a subset of a broader database that was generated using a validated finite element modeling

code [3-5]. The level of numerical noise in the AE signals obtained from the code is less by approximately three orders of magnitude than the typical out-of-plane displacement signal levels produced by the code.

Since real AE signals normally have significant electronic noise that is superimposed on the AE source-based signal, the purpose of the research reported here was to determine the effects of electronic (sensor/preamplifier-based) noise on the accuracy of WT-based arrival times. The finite element model results are ideal for such a study since the noise-free signals are available. This situation is not the case with experimental AE signals. Further, with experimental signals the exact location of the source is unknown, while for the finite-element signals the precise locations of the source and pseudo sensor(s) are known.

2. Finite Element Modeled AE Signal Database

The signal database used in the research reported here has been described in previous publications [1, 2, 6 and 7]. To provide a ready reference to key information, certain aspects are summarized here. The signals were generated by finite-element modeling (FEM) in an aluminum plate (1 m x 1 m x 4.7 mm). The AE signals represent the out-of-plane top-surface displacement as recorded by a perfect flat-with-frequency point-contact sensor. The AE signals were modeled for three in-plane propagation distances (60 mm, 120 mm and 180 mm from the source epicenter) and seven in-plane radiation angles (0° [x-direction], 12°, 22.5°, 45°, 67.5°, 78°, and 90° [y-direction]). All the FEM signals were numerically processed with a 40 kHz (four-pole Butterworth) high-pass filter followed by resampling from 44.6 ns/point to 0.1 μs/point. The AE signals were based on a 1.5 μs source rise time, and they were examined out to 150 μs after the source operation time. This procedure avoids the plate edge reflections, which appear well after the direct signals.

Table 1 provides pertinent information on the buried dipole-type AE sources used for a detailed examination of the effects of electronic sensor/preamplifier noise. Initially the study focused on data at a propagation distance of 180 mm and a radiation direction of 0˚. The six FEM cases described in the table were selected based upon the desire to include AE signal cases with the following features. First, an AE signal where its primary energy (as evaluated by a WT) was in the low frequency region of the fundamental antisymmetric Lamb mode. Second, a case where the primary signal energy was in the high frequency portion of the fundamental symmetric Lamb mode. Third, a case where the primary-signal energy was approximately equally distributed between these two portions of the fundamental modes. And fourth, additional cases so that each of the three selected source types was represented at two source depths. The source types selected were an in-plane dipole (aligned in the 0º direction), a microcrack initiation (with the primary dipole in the 0º direction), and a shear (without a moment) about the y-axis with the shear directions at 45˚ to the x and z axes. Previous research [1, 7] had identified the primary WT signal energy for this plate and these AE sources to be at the mode and key frequency combinations of A_0 at 60 kHz and S_0 at 522 kHz. Table 1 specifies the dominant mode and frequency combination(s) for each case of source type and source depth. The table also provides the relevant average group velocities [1, 7] and the ratio of the WT peak magnitudes (for each case) of the two mode and frequency combinations.

Table 1 Description of the source cases examined. [1, 7]

Case number	Source (depth in mm)	WT-based high intensity mode(s) and freq., kHz	Average group velocity, mm/μs	Ratio of noise-free WT peak magnitudes (A_0 at 60)/S_0 at 522 and (reciprocal)
9034	Shear w/o moment (0.783)	A_0 at 60	2.5	5.6 (0.18)
9004	Micro-crack initiation (1.41)	A_0 at 60	2.5	4.1 (0.24)
2793	In-plane dipole (1.723)	A_0 at 60	2.5	1.3 (0.77)
9002	Micro-crack initiation (2.037)	A_0 at 60 S_0 at 522	2.5 1.8	1 (1) 1 (1)
9030	Shear w/o moment (2.037)	S_0 at 522	1.8	0.41 (2.3)
2791	In-plane dipole (2.35)	S_0 at 522	1.8	No A_0 mode

3. Wavelet Transform Information

The WT results were obtained using the AGU-Vallen Wavelet freeware [8], with the key parameter settings being: maximum frequency = 700 kHz; frequency resolution = 3 kHz and wavelet size = 600 samples. The Wavelet Time Range Setting for the number of samples (i.e., points) was 1500. Thus, the signal was analyzed from the source operation time out to 150 μs. This allowed the full-direct-arrival signal to be transformed. The software automatically determines the arrival times of the peak WT magnitude at selected frequencies (for a 3-kHz wide band, starting at the selected frequencies of 60 and 522 kHz). The resolution of the arrival times was taken at 0.1 μs to correspond to the time resolution of the resampled FEM-based signals. The correspondence of the determined arrival times with the fundamental Lamb modes was facilitated by the software option that superimposed the group velocity curves on the WT results.

4. Description of Noise Signals and Creation of Modeled AE Signals plus Noise

To make the study of the effect of electronic noise as realistic as possible, the noise signals were obtained from a wideband high sensitivity conical sensor developed at NIST-Boulder [9, 10]. The noise signals were recorded at a preamplifier gain of 55 dB with the sensor coupled only to air and protected by soft foam from any airborne signals. A total of ten noise signals were available. Each signal had been digitized by a 12-bit waveform recorder with a sampling interval of 0.1 μs per point, which corresponded to the resampled FEM signals. Each signal was about 16000 points in length, which resulted in the ten signals representing a total of about 16 ms of noise. The typical crest factor of the signals was 4.2. A typical time domain and Fast Fourier Transform (FFT) from one of these ten signals is shown in Fig. 1. The slightly smoothed FFT was calculated after the signals had been numerically bandpass filtered (six-pole Butterworth) from 40 kHz to 1.2 MHz. This filter was used to make all the noise signals more representative of the frequency range of the FEM signals. After modifying the noise signal amplitudes (so they were less than the FEM signal amplitudes) and changing the units to picometers, the signals were examined to determine their consistency. First, the peak magnitudes for the 10 noise signals were determined. The mean peak magnitude was found to be 0.63 pm with a dispersion of 10 % and a range of 0.54 to 0.73 pm. Thus, the different noise signals were considered to be relatively uniform in their peak signal magnitudes.

Figure 2 shows the WT result of about an 800 μs portion of a typical noise signal. Figure 3 demonstrates typical plots of the noise WT magnitude versus time at each of the two key

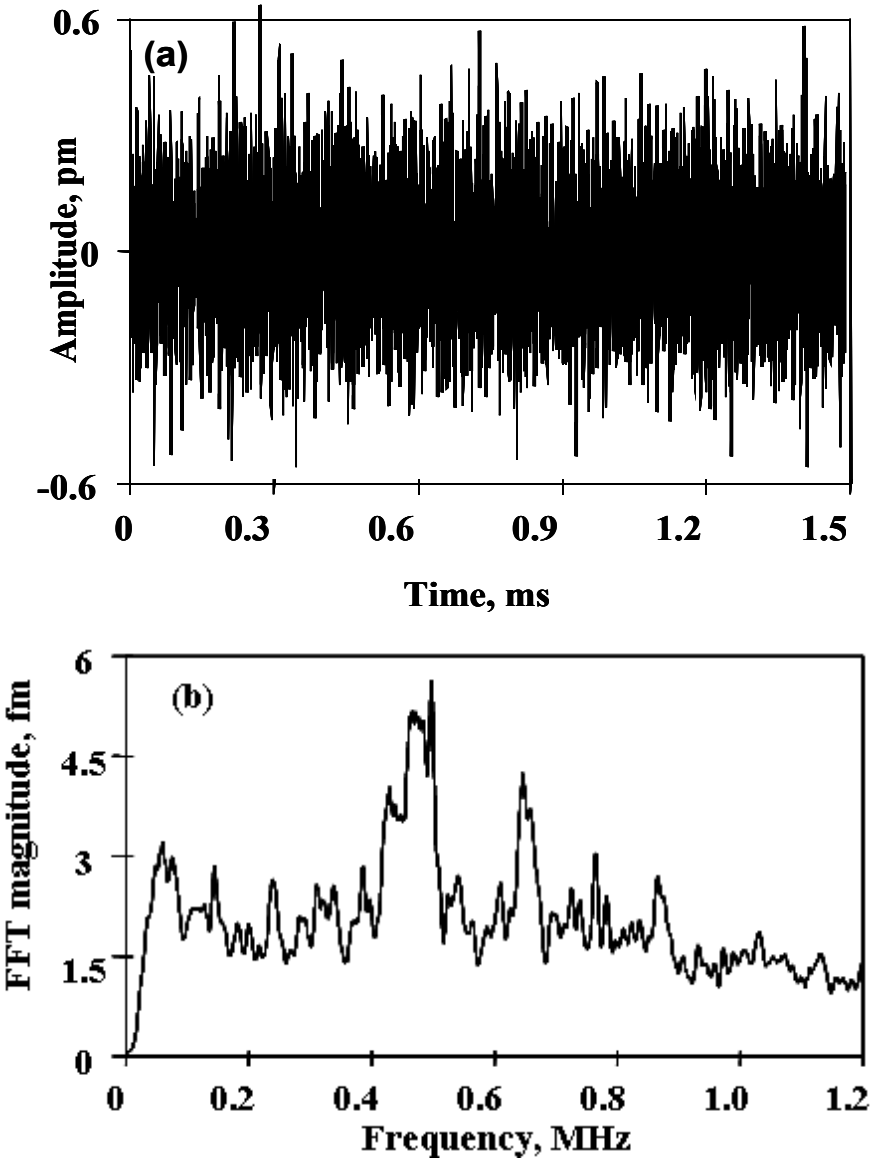

Fig. 1 Time domain (a) and FFT (b) of a typical noise signal (after a gain of 55 dB) of 16384 points at 0.1 μs/point.

frequencies. It is clear from this figure that the WT magnitude versus time varies over a wide range for each of the two key frequencies. The figure also shows that the number of fluctuations of the WT magnitudes increases with increasing frequency (likely a characteristic of the WT used in this research). Further, the WT magnitude variations in Fig. 3 indicate that, when noise is added to the FEM-generated AE signals, the WT peak magnitudes of the signal plus noise (S+N) could experience noise-induced modifications. Since, for real-world AE signals, the amplitudes of the WTs of the underlying noise signal at the times of mode arrivals would be a random and unpredictable condition, a statistical study of noise effects on arrival times was necessary.

To form a suitable noise database for a statistical study, a total of 50 different noise segments, each nominally 160 μs in length, was extracted (after the filtering and amplitude change, as described above) from the modified database of ten noise signals. A S+N database was then constructed for the selected FEM cases (source type and depth) of interest. For each case the same 50 noise signals were added to the FEM-based (noise-free) AE signal to form a database of

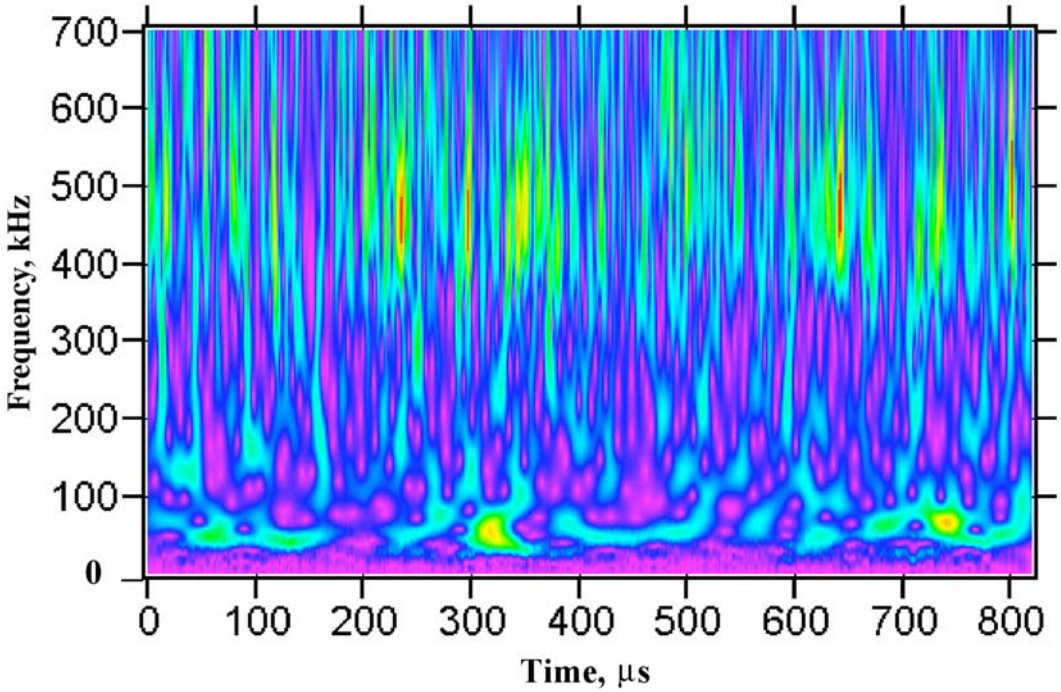

Fig. 2 Wavelet transform of a 819.2 μs portion of a typical noise signal. Color (maximum is red) or contrast shows WT intensity

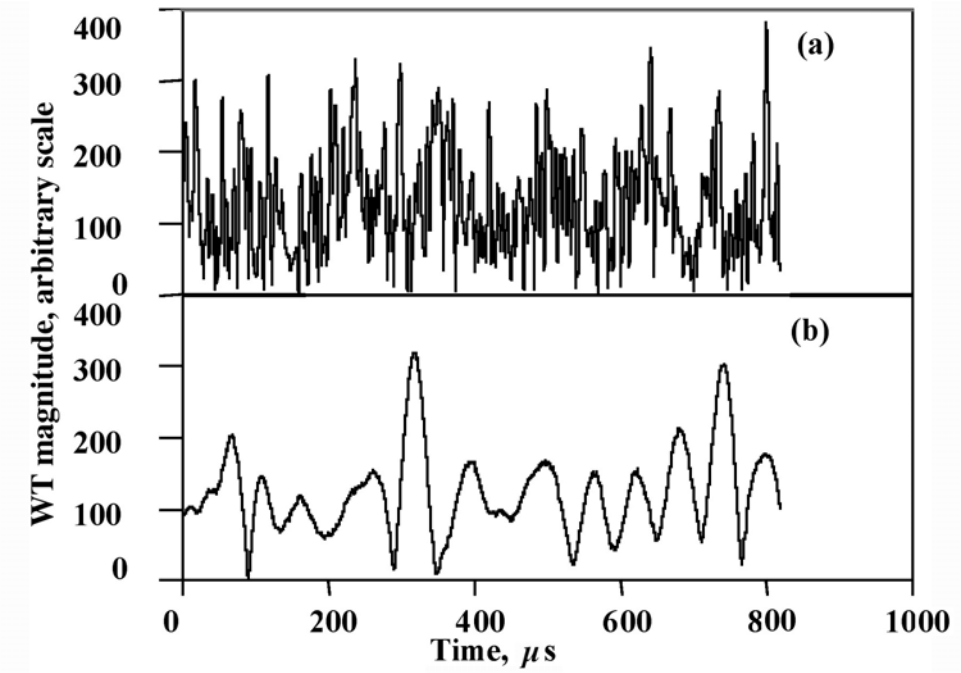

Fig. 3 Magnitude of wavelet transformation (a) at 522 kHz and (b) at 60 kHz versus time for a typical 819.2 μs noise signal.

50 S+N signals. Before adding the noise signals they were multiplied by a factor to obtain a certain S/N ratio. This S/N ratio was based on the peak amplitude of each noise-free FEM signal and the mean peak amplitude (0.63 pm) representative of all the noise signals. The 50 S+N signals were called a "set" of S+N signals for a given FEM signal case. In order to be able to directly track the effects of different S/N ratios applied to the same FEM-based noise-free signals,

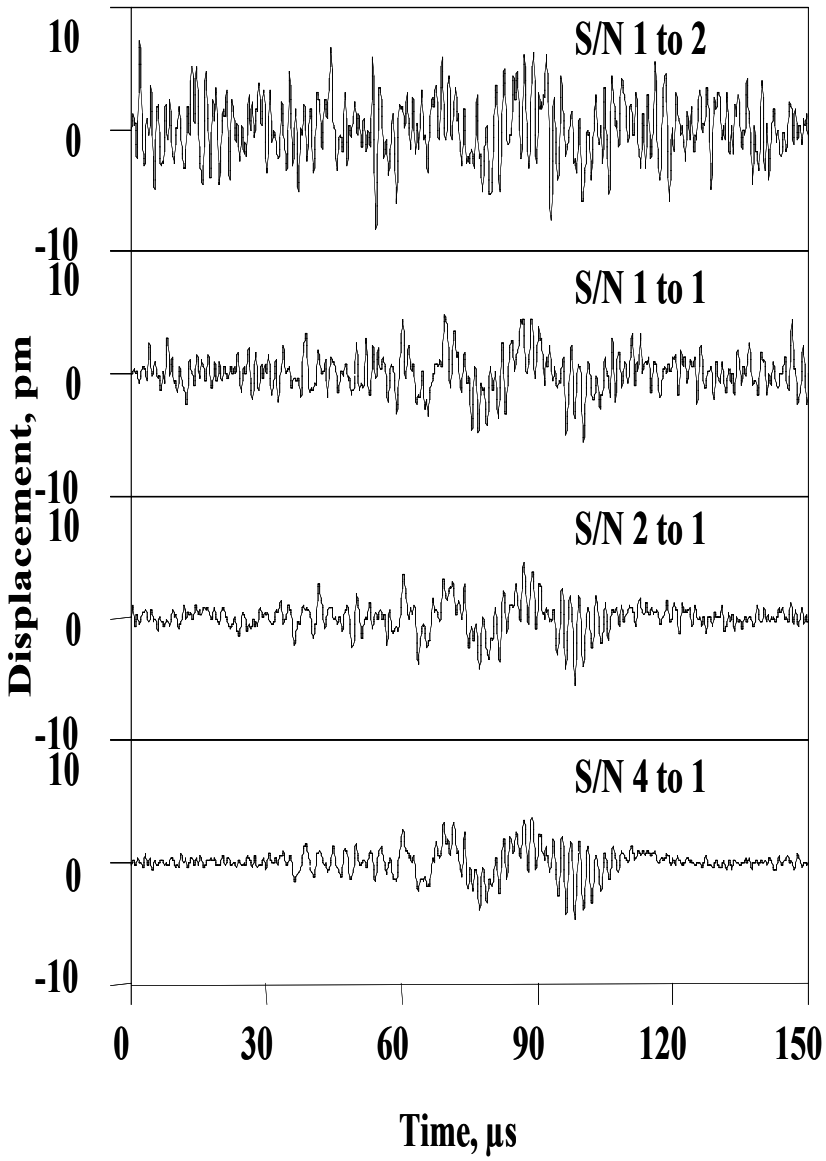

Fig. 4 Typical examples of S+N signals for case 2793 at four different S/N ratios.

the same sequence of noise signals (multiplied by a different factor to create a different S/N ratio) was added respectively to the noise-free signal to form each "set" of S+N signals. WTs of the S+N signals were then carried out for each case for the different S/N ratios, and the appropriate arrival times were obtained. Figure 4 shows examples of the S+N signals for case 2793 at four different S/N ratios.

5. Effects of Electronic Noise on WT-Determined S+N Signal Arrival Times (at a propagation distance of 180 mm in the zero-degree radiation direction)

For each case (AE source type, source depth and S/N ratio), a total of 50 arrival times at the mode and frequency combination(s) (shown in Table 1) was obtained from the WT results. The 50 arrival times represent the effect of the random variation in the noise. Table 2 shows a statistical characterization of the arrival times as a function of the S/N ratio for one source type and depth (case 2793; see Fig. 4). The table provides the average arrival time, maximum time, minimum time and sample standard deviation (SD), as well as the noise-free arrival time. Even

Table 2 Statistical characterization of 50 arrival times for the in-plane dipole source (case 2793) as a function of the S/N ratio for 180 mm propagation distance and at 0° radiation direction.

S/N Ratio	Avg., μs	Max., μs	Min., μs	SD, μs	Noise-free time, μs
1 to 2	81.2	113.7	73.6	8.2	78.2
1 to 1	77.4	80.7	73.8	1.6	78.2
2 to 1	77.9	78.8	75.6	0.8	78.2
4 to 1	78.2	78.4	77.7	0.1	78.2

Table 3 The average and standard deviation (50 samples) of the arrival times for all the cases in Table 1 for 180 mm propagation distance at 0° radiation direction.

Case number and frequency, kHz	Avg. arrival time and SD, μs with S/N at 1 to 2	Avg. arrival time and SD, μs with S/N at 1 to 1	Noise-free arrival time, μs
9034 (60)	77.4 (2.2)	77.5 (1.1)	77.9
9004 (60)	77.4 (1.9)	77.6 (1.0)	78.0
2793 (60)	81.2 (8.2)	77.4 (1.57)	78.2
9002 (60)	78.4 (13)	77.5 (1.9)	78.2
9002 (522)	87.7 (28)	98.1 (4.2)	98.2
9030 (522)	94.2 (15)	98.1 (1.63)	98.0
2791 (522)	92.6 (17)	98.7 (1.55)	98.0

at an S/N ratio of 1 to 1, the maximum and minimum times of 80.7 μs and 73.8 μs are not large deviations from the noise-free value of 78.2 μs. To justify the conclusion that these maximum and minimum times are not large, a threshold-based determination of possible arrival times was made for the relevant noise-free signal. Since the threshold method depends on the actual threshold used, a range of thresholds was used (equivalent to varying AE source signal amplitudes with a fixed threshold). The range of arrival times determined was from 32.9 μs to 75.2 μs. This range of 42.3 μs is clearly much larger than the WT-based range of 6.3 μs at the 1 to 1 S/N ratio. We note again that the WT method is independent of threshold. Thus the threshold-based method would likely lead to significant location errors compared to the WT approach.

Table 3 shows the average and sample standard deviations (SDs) of the arrival times for all the cases (listed in Table 1) at two S/N ratios (1 to 2 and 1 to 1). The results at two additional S/N ratios (2 to 1 and 4 to 1) were nearly identical to the noise-free values as is illustrated for one case in Table 2. Thus those results are not shown here. Compared to the noise-free arrival times, the average values are quite close to the noise-free values, even at an S/N ratio of 1 to 2.

6. Discussion of Above Results

In subsequent discussions, the evaluation of the magnitude of noise-based arrival time errors was based on comparisons of the sample SDs. The decision to use this measure arose from the observation that smaller SDs indicated that the arrival times were tightly grouped around the mean values. As Table 3 shows, the mean values at an S/N ratio of 1 to 1 were all very near the noise-free arrival times. We assert that the smaller the SDs, the smaller the range of noise-induced arrival time errors and the smaller the subsequent location errors.

Examination of the results in Table 3 leads to the interesting observation that the SDs are the largest for case 9002 for each of the two key frequencies and for each S/N ratio. As can be seen in Table 1, the FEM-based noise-free signal for this case exhibited significant energy (in the WT magnitude results) at both key frequency and mode combinations. This observation implies that when the noise-free AE signal energy is significant in more than one mode, then errors in WT-based arrival times will be greater than when the signal energy is predominantly in a portion of a single mode. This conclusion is consistent with the fact that when the FEM displacement signal amplitude is determined by two modes, the WT peaks from those individual modes will be smaller relative to the WT magnitudes of the noise as compared to the case where the FEM signal is significantly dominated by a single frequency/mode. This conclusion is also consistent with the fact that the S/N ratio was related to the time domain, while the WT-based results come from a time *and* frequency domain.

An important question relates as to whether the type of source changes the accuracy of WT-based arrival times when noisy signals are examined. If the information in the last column in Table 1 is considered in relation to the SDs of the arrival times (see Table 3) at an S/N ratio of 1 to 1, there is a correlation. In particular, the greater the dominance of the noise-free peak WT magnitude of the dominant frequency/mode combination, the smaller the SDs. The converse applies the smaller the dominance. As with case 9002 above, this result is related to the fact that the S/N ratio is from the time domain, and the arrival times are from the frequency/time domain. Hence at a certain S/N ratio, strong single-mode dominance means that a greater proportion of the WT magnitude comes from the source-based signal relative to the WT magnitude contribution from the noise. The WT contribution from the noise does not depend on the source type, while that from the source-based signal can be from one or two modes. Thus, it is not the source type, but the magnitude of the modal dominance in the displacement signal, that is significant. Previously published work [2, 6] has shown that the modal dominance is directly related to the depth of the point source below the plate surface, and that the source type typically has only a minor effect on the relative magnitudes of the modes generated.

When the frequency dependence of the results in Table 3 was examined at the S/N ratio of 1 to 2, it is found that the SDs were the largest for the cases where the 522 kHz/S_0 mode dominates. This conclusion was not surprising considering the typical FFT spectrum of the noise demonstrated in Fig. 2. The figure shows a region of higher noise near this frequency. To quantify the WT magnitude difference of noise between the two frequency bands (3 kHz wide) the 50 noise signals were studied. The WT peak magnitudes at both 60 and 522 kHz were obtained over a signal length of 150 μs. The average (for 50 samples) WT peak values at each frequency were obtained and their ratio was found. The average 522 kHz WT peak magnitude was found to be 1.6 times the average for the 60 kHz WT peak. This result implies that the peak regions of the noise spectrum can be used to predict the frequencies where the noise will likely result in the largest errors in WT-determined arrival times.

7. Effects of Radiation Angle (at a propagation distance of 180 mm)

To specifically examine the effects of radiation angle on the accuracy of WT-based arrival times for signals with noise, it was decided to ignore changes in signal amplitudes as the radiation angle changed from zero to 90 degrees. Thus the S/N ratios (for this examination) were calculated based on the signal peak amplitude in the specific radiation direction under consideration. Hence, the arrival time errors at radiation angles other than zero could be directly compared

at the same S/N ratio with the results for the zero-degree radiation direction. Only three cases were chosen to examine the effects of radiation angle. This decision was based on the fact that in the previous section all the trends were apparent within the results for cases 9002, 9004 and 9030 (selected from Table 1).

In review, case 9002 provided a case where both frequency and mode combinations were significant. And cases 9004 and 9030 provided examples where the 60 kHz/A_0 and 522 kHz/S_0 combinations respectively had a strong dominance. The S/N ratio considered was limited to 1 to 1 since in the above section the major trends were apparent at this ratio. In addition, to compare with the above section results, the propagation distance was limited to 180 mm.

Table 4 The standard deviation (50 samples) of the arrival times at two different angles for 180 mm propagation distance and an S/N ratio of 1 to 1.

Case number and (frequency, kHz)	SD, μs at zero deg.	Ratio: noise-free WT peak at indicated freq./alt. freq. value at 0˚	SD, μs at 45˚	Ratio: noise-free WT peak at indicated freq./alt. freq. value at 45˚	SD, μs at 67.5˚	Ratio: noise-free WT peak at indicated freq./alt. freq. value at 67.5˚
9004 (60)	0.99	4.1	------	------	0.96	33
9002 (60)	1.9	1.01	1.3	1.5	------	------
9002 (522)	4.2	0.99	12	0.68	------	------
9030 (522)	1.6	2.3	------	------	1.7	3.2

Table 4 shows the arrival time sample SD results at angles greater than 0˚ for 50 samples at an S/N ratio of 1 to 1 along with the results at the 0˚ angle to allow a direct comparison. The results indicate that the SD at the larger angle is about the same as the value at the zero-degree radiation angle when a strong dominance of one mode and frequency combination is present. But in case 9002, where both combinations had significant magnitudes, the SD results differed at the larger angle compared to those at the 0˚ angle. In particular the arrival time errors had a higher SD at 45˚ compared to the SD at 0˚ for the 522 kHz/S_0 mode, while the arrival time errors had a lower SD at 45˚ for the 60 kHz/A_0 mode compared to the 0˚ direction. This observation is consistent with the discussion in the previous section about the effect of the level of dominance of the frequency/mode combinations. When the noise-free WT peak magnitude ratio of 60 kHz/A_0 over 522 kHz/S_0 was calculated, the ratio at 0˚ was 1, and at 45˚ it was 1.5 (see Table 4). Thus, due to the source radiation characteristics, the 60 kHz/A_0 mode content of the signal increases at the larger radiation angle, while the 522 kHz/S_0 mode content decreases. Hence the noise has a smaller effect on the arrival error results for the 60 kHz/A_0 mode, and the converse applies for the 522 kHz/S_0 mode at the larger radiation angle. These results indicate that, as a general conclusion, the dependence (at a certain S/N ratio) of arrival time errors on radiation angle will again depend on the level of dominance of the dominant frequency and mode combination as the radiation angle varies.

8. Effects of Propagation Distance (in the zero-degree radiation direction)

Since it is well known that the amplitude of AE signals falls off with increasing propagation distance, the same philosophy used for the radiation angle study was used in the examination of

the effect of propagation distance. Namely, the noise levels were adjusted such that at each propagation distance the actual S/N ratio was the same. Hence, direct comparisons at the same S/N ratio could be made at the different distances. For all of the cases in Table 1 the arrival times at the 60 and 120 mm propagation distances (0˚ radiation direction) were determined from the WT-based technique at two S/N ratios: 1 to 2 and 1 to 1. As before, it is most insightful to make comparisons using the SDs of the arrival times that were determined for the 50 trials for each case. Table 5 shows the SDs for an S/N ratio of 1 to 1 at these two distances along with the previously documented results from 180 mm (Table 3).

Table 5 The standard deviation (50 samples) of the arrival times at three different propagation distances for the 0˚ propagation direction and S/N of 1 to 1.

Case number and (frequency, kHz)	SD, μs at 60 mm and rank* ( )	SD, μs at 120 mm and rank* ( )	SD, μs at 180 mm and rank* ( )
9034 (60)	1.5 (4)	1.0 (2)	1.1 (2)
9004 (60)	1.6 (5)	0.74 (1)	0.99 (1)
2793 (60)	3.0 (6)	1.51 (5)	1.57 (4)
9002 (60)	5.8 (7)	5.3 (7)	1.9 (6)
9002 (522)	1.3 (3)	3.0 (6)	4.2 (7)
9030 (522)	0.84 (1)	1.45 (4)	1.63 (5)
2791 (522)	0.97 (2)	1.2 (3)	1.55 (3)

*Lowest S/N is rank (1)

Table 6 Ratios of noise-free WT peak magnitudes (dominant magnitude in the numerator) at the two key frequencies as a function of propagation distance in 0˚ direction.

Case number	At 60 mm, dominant frequency (kHz) shown	At 120 mm, dominant frequency (kHz) shown	At 180 mm, dominant frequency (kHz) shown
9034	4.3 (60)	5.0 (60)	5.6 (60)
9004	3.1 (60)	3.4 (60)	4.1 (60)
2793	1.0 (522)	1.2 (60)	1.3 (60)
9002	1.3 (522)	1.1 (522)	1.0 (60)
9030	3.0 (522)	2.5 (522)	2.4 (522)
2791	N.A.*(522)	N.A.*(522)	N.A.*(522)

* No A_0 mode present

To facilitate the discussion of the effects of propagation distance on the SDs, the results in Table 5 at each distance have been numerically ranked from the best (1) with the lowest SD to the worst (7) with the largest SD. In order to try to "break" ties, extra decimal places have been shown in some cases. Clearly the order changes at the 1 to 1 S/N ratio as the propagation distance changes. Some general trends in Table 5 can be associated with the relative level of dominance of the modes. Table 6 shows how the ratios of the two WT peak magnitudes of the noise-free signals varied for the different source cases and propagation distances along the 0º direction. When the 60 kHz/A_0 mode dominates, the ratio is (60 kHz/A_0 mode magnitude)/(522 kHz/S_0 mode magnitude). For each case, the changes in the ratios only show the effect of the propagation distance. Table 6 clearly shows the relative peak WT magnitudes for the 522 kHz/S_0 mode fall off with increasing propagation distance (Cases 9002 and 9034). In contrast, Cases 9034 and 9004 show the relative 60 kHz/A_0 mode peak WT magnitudes increasing with distance. A proposed cause for this effect will be discussed in the next section.

Based on the results in Table 6, we note that the ranking in Table 5 (at a certain propagation distance) of the best to worst SD for each frequency and mode generally correlates with the amount of relative dominance of that frequency/mode regardless of the propagation distance. For example at 60 mm, the best SD for case 9034 has a strong dominance for the 60 kHz/A_0 mode (4.3, see Table 6), and the worst SD for case 9002 is actually dominated by the 522 kHz/S_0 mode (1.3, see Table 6). Table 6 also provides a reason for the SD ranking (in Table 5) changing with the propagation distance. The increase in 60 kHz/A_0 mode dominance (see Table 6) with increasing distance correlates with the observation that at the larger propagation distances the 60 kHz/A_0 mode generally has the best SDs, except for one case (we ignore case 9002 since both modes have about the same peak magnitude). The results for case (2791) rank as one of the best at all the propagation distances due to the fact that the dominance of the 522 kHz/S_0 mode is very strong since there is no A_0 mode for this midplane source.

A question arises, why are the 522 kHz/S_0 mode results the best at the 60 mm distance even though there are two 60 kHz/A_0 cases (9034 and 9004) with strong dominance? The answer to this question is likely due to the "spreading in time" of the WT results at lower frequencies. The "spreading in time" terminology refers to the signal at a specific time contributing to the WT magnitudes over a range in time about that specific time. This characteristic at lower frequencies is illustrated in Fig. 5. In this figure the input signal to the WT is a Dirac delta function. Thus we suggest the 60 kHz/A_0 mode WT peak magnitude arrival time has larger errors since the WT peak magnitude in that case reflects a wider time-range of the noise signal (see Fig. 5). In contrast, the 522 kHz/S_0 mode WT magnitude does not have the same range of arrival time errors because the WT peak magnitude at that frequency does not result from as wide a time range of the noise signal. At the longer propagation distances, the drop in the dominance of the 522 kHz/S_0 mode is evidently sufficient to allow the higher magnitude noise in the region of 522 kHz (see Fig. 2) to increase the SDs. This results in the 60 kHz/A_0 mode SDs being generally the lowest at the longer distances.

9. Relative Fall-off of the 522 kHz/S_0 Mode with Increased Propagation Distance

The 522 kHz/S_0 mode falls-off at a faster rate than the 60 kHz/A_0 mode with increasing propagation distance as is shown in Table 6. Since the finite element modeling results did not incorporate the available frequency-based attenuation with propagation distance, the source of this frequency/mode fall-off is of interest. Since the frequency band is only 3 kHz wide in the WT computation, there should not be much dispersion with increasing propagation distance. To check this assumption, the profile of the WT magnitude (at each of the two frequencies) as a function of time was plotted for one of the cases (case 9002, noise-free signal) at the three propagation distances. The normalized results in Fig. 6 show some potential dispersion for the 522 kHz/S_0 mode. For example, at 60 % of the peak magnitude of the 522 kHz profile (in the largest magnitude peak region) the width of the profile increases by 50 % as the propagation distance increases from 60 mm to 180 mm. On the other hand, the change of width over those propagation distances at this level was not perceptible for the 60 kHz mode. It is suspected that this fall-off can be attributed to the following observations. In the 522 kHz region of the S_0 mode, the group velocity curve makes nearly a "U-turn" (see Fig. 1 in reference 1) in the group velocity direction over a limited range of frequency change. Thus a range of frequencies in this region have about the same group velocity. This feature, in combination with the characteristic of the WT described next, likely causes this attenuation.

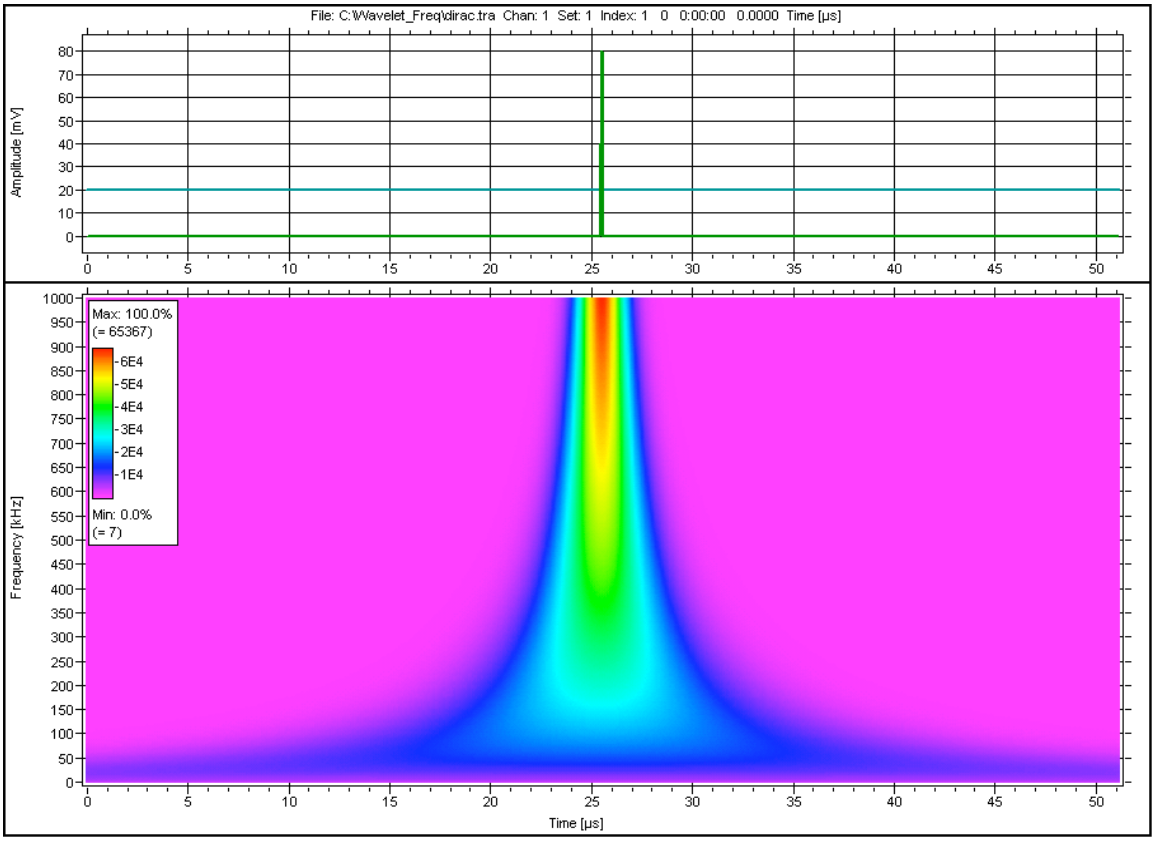

Fig. 5 WT result with input signal of a Dirac delta function (amplitude in mV) as shown in the upper time domain. Vertical frequency scale of WT result (lower part of figure) from 0 to 1 MHz and time scale of both plots 0 to 51.2 µs. Color or contrast shows the WT magnitude.

Figure 7 shows that the WT used in this research has the characteristic of its magnitude "spreading in frequency" at higher frequencies. This "spreading in frequency" means that the signal at a specific frequency contributes to the WT magnitudes over a range of frequencies about the specific frequency. This effect does not appear in Fig. 7 at lower frequencies. The WT shown in Fig. 7 was created from a time-domain signal that was made up of a sinusoidal signal that has a change in frequency from 60 kHz to 522 kHz, as is shown in the top portion of the figure. The two sinusoidal portions of the time-domain signal had equal amplitudes, yet the WT result has significantly lower peak magnitude (only about 36 % of the 60 kHz value), with obvious "spreading in frequency" for the sinusoidal portion of the signal at the single frequency of 522 kHz. Thus it seems likely that the combination of the "spread in frequency" and the "U-turn" results in the "attenuation" of the 522 kHz/S_0 WT peak magnitude with increasing propagation distance. Thus the supposed dispersion-based "attenuation" is really related to the characteristics of the WT used in this research in combination with the shape of the group velocity curves in a particular region.

10. Location Errors versus S/N Ratio

The statistical properties discussed above do not directly address the important issue raised by the potential for noise to alter WT-based signal arrival times. The central issue concerns the effect of arrival time errors on the accuracy of the calculated AE source location. To address this question, a decision was made to focus on linear location. This choice was based on a desire to

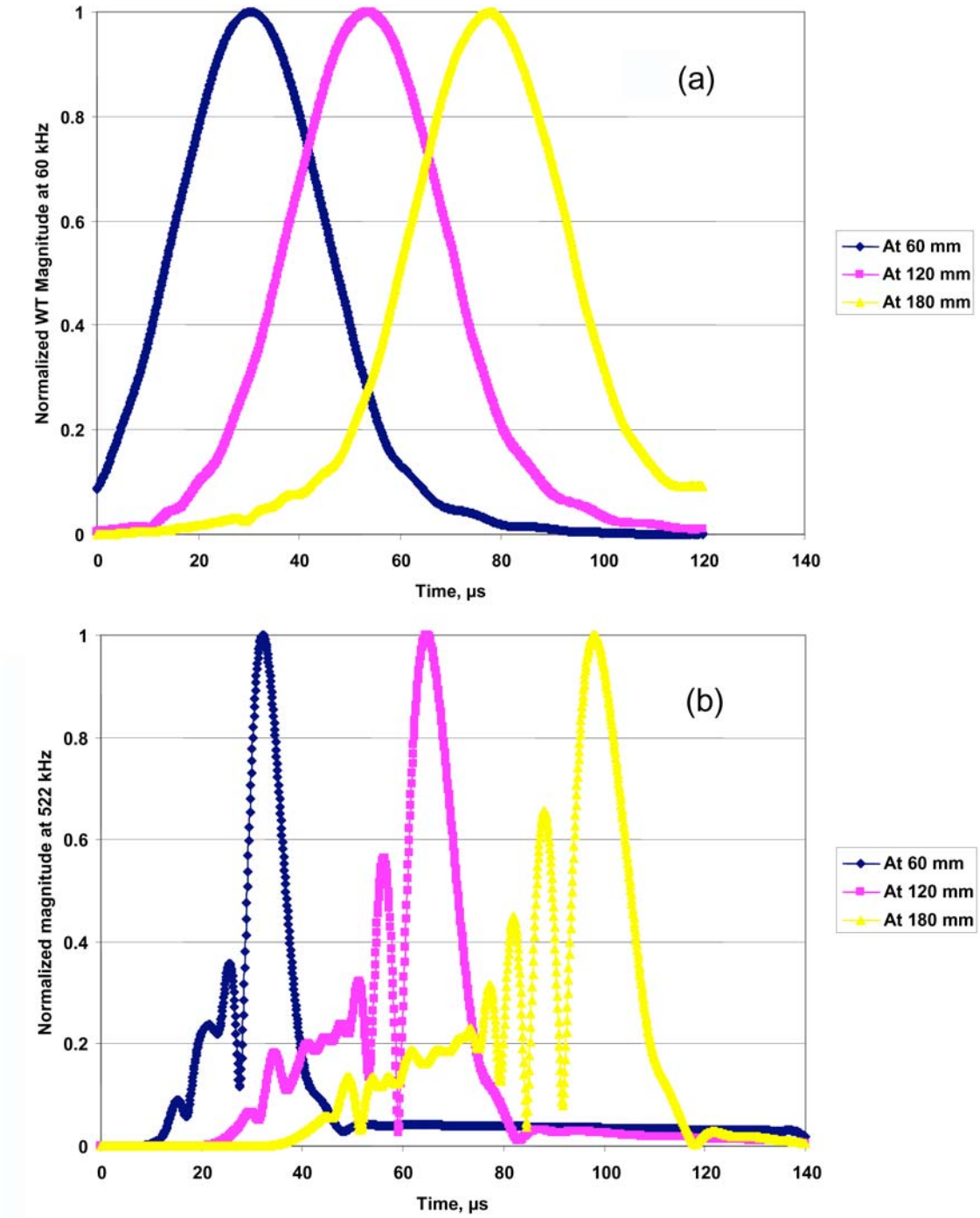

Fig. 6(a) Profile of WT magnitude at 60 kHz versus time and (b) profile of WT magnitude at 522 kHz versus time, both for case 9004.

remove any dependence of the location error-analysis results on the particular computational scheme used for two-dimensional location calculations. Figure 8 shows a schematic of the linear location geometry and the notation used in this paper. Straightforward manipulation of the governing equations leads to the following:

$$d_1 = 0.5\,[d - c_g\,(t_2 - t_1)], \quad (1)$$

$$d_2 = 0.5\,[d + c_g\,(t_2 - t_1)], \quad (2)$$

$$d = d_1 + d_2, \quad (3)$$

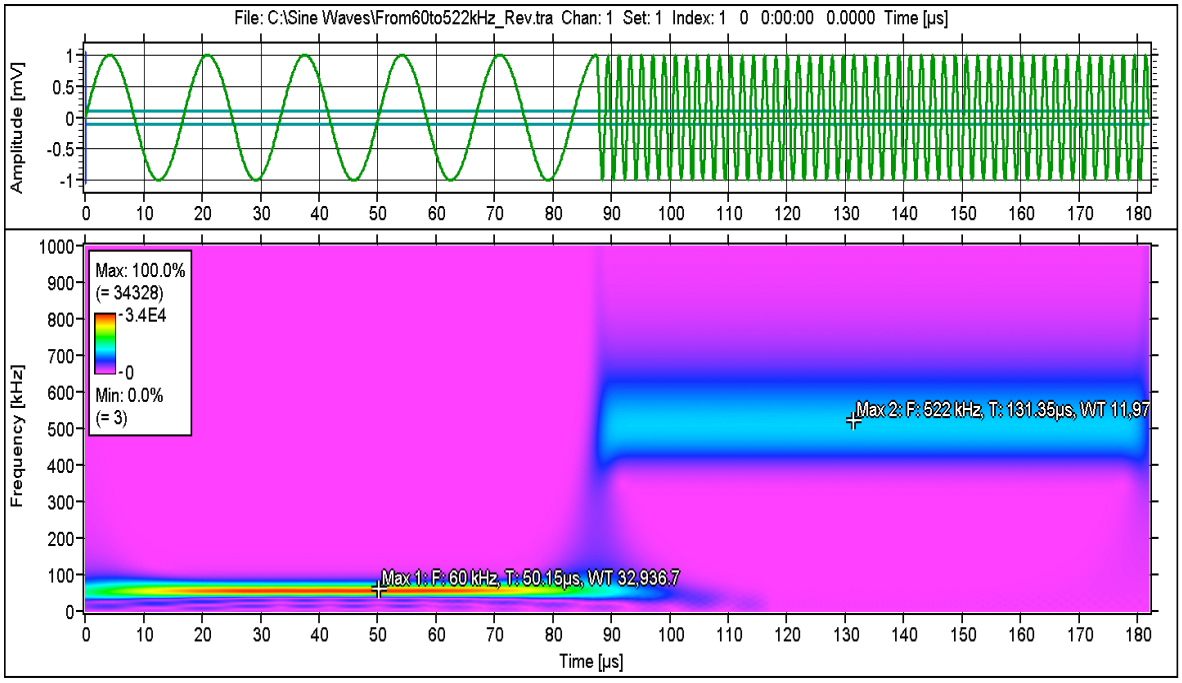

Fig. 7 Signal and WT of the signal. Signal is 60 kHz sine wave followed by 522 kHz sine wave of same amplitude. WT maximum magnitudes of 32,937 and 11,970 for 60 kHz, and 522 kHz portions of WT.

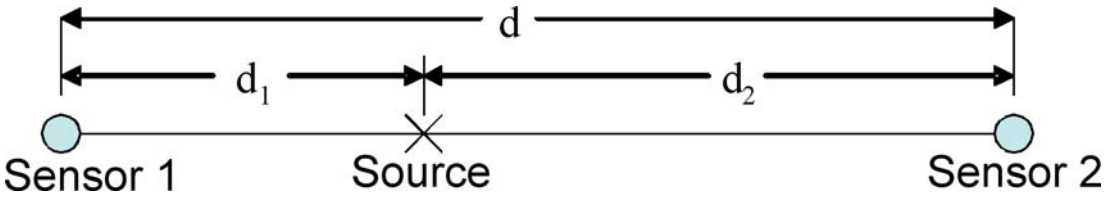

Fig. 8 Geometry for linear location equations.

where c_g is the appropriate group velocity, d is the sensor spacing, d_1 is the distance from the first hit sensor to the source location, and d_2 is the distance from the second hit sensor. The values t_1 and t_2 are the respective arrival times. To allow the analysis to focus directly on arrival time errors due to the addition of noise, it was decided to consider geometry where the source was equally spaced between the two sensors. With this approach, when two different S+N signals (associated with the same noise-free case) are used to calculate a location, the location error will be directly due to noise-altered arrival times. When noise is present, equations (1) and (2) can be rewritten (with italics to denote the values when noise is present) as:

$$d_1 = 0.5\ [d - c_g\ (\pm e)], \quad (4)$$

$$d_2 = 0.5\ [d + c_g\ (\pm e)], \quad (5)$$

where $e = |t_1 - t_2| > 0$ is the arrival *time-difference* error. On an absolute value basis the percent location errors in d_1 and d_2 values are equal, and this error is given by

$$\text{percent error} = [(c_g \cdot e) / d] \times 100\ \%. \quad (6)$$

To form databases of time differences for each case (source type, depth and S/N ratio) the 50 arrival times obtained from each "set" were used in the following fashion. The absolute value differences of the first arrival time and each of the subsequent 49 values was determined.

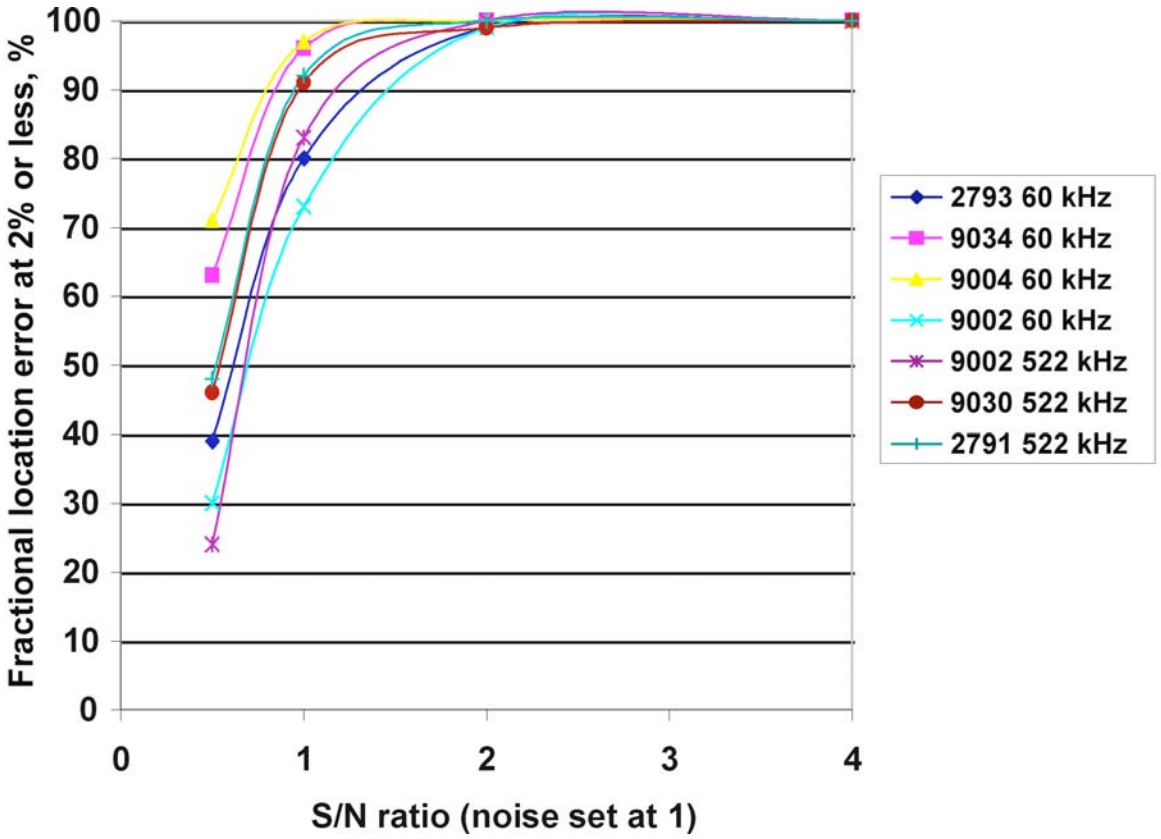

Fig. 9 Fraction (%) of the 1225 calculated locations with an error of 2 % or less as a function of the S/N ratio for all cases (source type and depth).

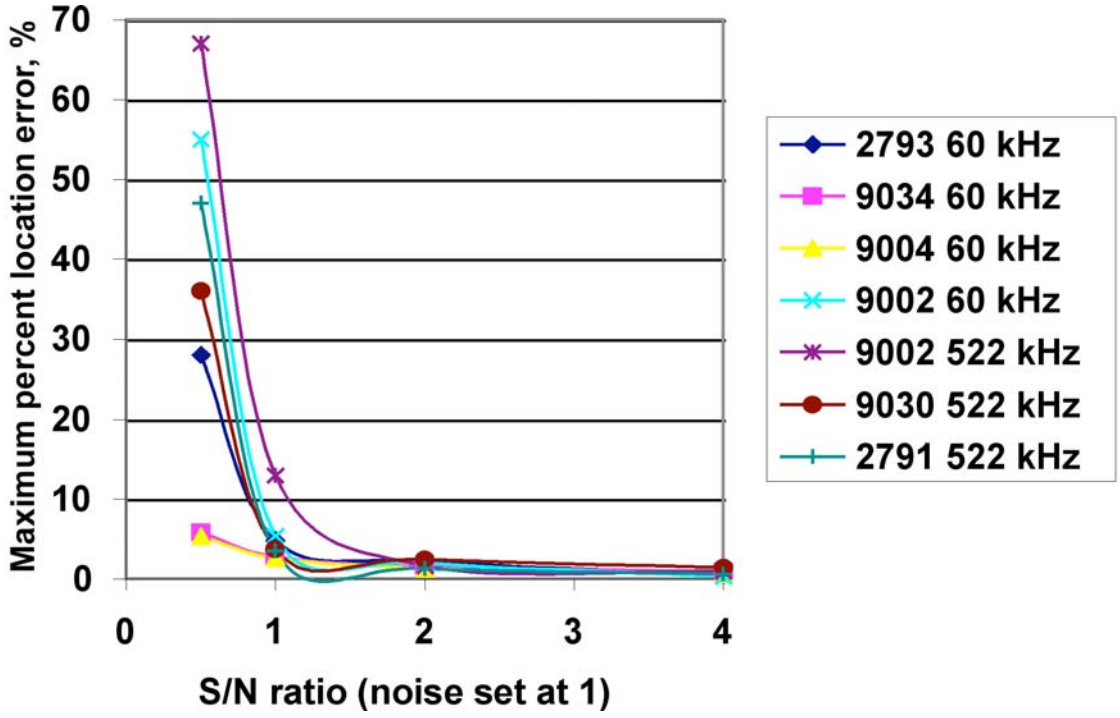

Fig. 10 Maximum location error (%) for the 1225 calculated locations for all cases as a function of the S/N ratio (Note that the dip in the curves between S/N ratios of 1 to 2 is an artifact of the plotting routine).

Then the absolute value differences of the second arrival time and each of the subsequent 48 values were determined. This process was continued in a similar fashion so that a total of 1225 arrival time differences were obtained for each case. These differences correspond to the *e* values in equation (6). By use of equation (6), the location errors were determined for each of the 1225 arrival time differences. Figure 9 shows as a function of the S/N ratio, the percentage of the 1225 trials for each case when the location error was 2 % or less based upon the sensor spacing (360 mm) for a nominal propagation distance of 180 mm in the zero-degree direction. In addition, Fig. 10 illustrates the maximum location error found in the 1225 trials for each case as a function of the S/N ratios.

The data illustrated in Fig. 9 demonstrates that even with an S/N ratio of 1 to 1, at least 73 % of the 1225 location calculations for each case resulted in a location error that was 2 % or less. Further, Fig. 10 shows the maximum location error for the 1225 location calculations for each case was 13 % or less. To appreciate these results, it should be pointed out that a typical fixed-threshold AE system would not even trigger on any of these signals because the required low threshold would trigger on multiple noise spikes. Hence, the technique used here could be of value for an AE acquisition system that records continuously.

At a 2 to 1 S/N ratio, Fig. 9 shows that at least 99 % of the 1225 location calculations for each case would have location errors of 2 % or less. Figure 10 also shows the maximum location errors would be 2.4 % or less. With an S/N ratio of 2 to 1, a fixed-threshold AE system would likely trigger on real AE signals instead of noise spikes. And for a source equidistant between the sensors, the location errors would not be great. The reason is that the factors of geometric attenuation, dispersion, and variations in source amplitude would be the same for the signal at both sensors. But for a fixed-threshold system, when the source is not equidistant from all the sensors, the above three factors would typically result in relatively large location errors compared to the 2 % location error limit used in this research. On the other hand, the WT-based determination of arrival times would not be affected by the above three factors.

11. Discussion of Location Error Results at a 180-mm Propagation Distance

To better appreciate just how good the above location results are the following facts must be considered. The noise level was taken at the average peak value of the original set of ten noise signals. If it had been set at the peak value (0.73 pm) of the ten signals, then the S/N ratios of 1 to 1 and 2 to 1 would have been 0.86 to 1 and 1.73 to 1. Even these S/N ratios are conservative values from the view of a typical AE experimentalist, since the peak was that for only about 16 ms of noise signal data.

The analysis presented in equations (1) through (6) predicts that the error in the location should depend linearly on the group velocity, c_g. Clearly Figs. 9 and 10 do not support that conclusion. The lower group velocity of 1.8 mm/μs for 522 kHz/S_0 does not give the expected better results. This lack of dependence on c_g is likely due to the previously discussed high noise-signal energy in the region of the 522 kHz frequency. This higher noise was evidently sufficient to overcome the expected dependence on c_g.

For further discussion of the location results, it makes the most sense to focus on the fraction of the 1225 trials that resulted in location errors of 2 % or less. The reason for this focus is that these results represent the average results over many trials. In contrast, the results of the

maximum location error represent only the worst case out of the 1225 trials for each source case and S/N ratio.

With this focus, we can examine in more detail the cases that give the best and worst results for the fraction of trials with location errors of 2 % or less. In each case it will be shown that the same facts apply that explained the general trends of the ordering of the results by SDs of the arrival times for these cases. Hence these discussions will not be as detailed as they were in the discussions of arrival times.

If the order of the best (highest fraction with small location errors) to worst results in Fig. 9 (at 0˚, 180 mm and S/N ratios of 1 to 2 and 1 to 1) is examined, the best results are for the cases with a strong dominance of the 60 kHz/A_0 mode (9004 and 9034) trailed by the results for the strong dominance of the 522 kHz/S_0 mode (2791 and 9030). The reasons for the cases with strong single mode dominance being best were already described in the discussion of arrival time results. In addition this ordering of the results relates to the "attenuation", as discussed previously, of the 522 kHz/S_0 mode with propagation distance. This attenuation increases the dominance of the 60 kHz/A_0 mode at a propagation distance of 180 mm. The worst location error results are for the cases (9002 and 2793) where both frequency/mode combinations are significant in the noise-free signals. In these cases, as previously described, neither mode overpowers the noise. The case (2791), which has a strong dominance of the 522 kHz/S_0 mode, is not among the best due to the extra noise in the vicinity of that frequency.

12. Location Error Effects of Propagation Distance and Radiation Angle

To examine the effect of propagation distance on source location errors, one must consider Fig. 11. This figure shows the fraction of trials with errors in location less than or equal to 2 % at the propagation distances of 60, 120, and 180 mm for S/N ratios of 1 to 1 and 2 to 1. The first observation is that the percentage of the 1225 trials with small location errors increases with increasing propagation distance. This result is not unexpected since the calculation of the location error has the sensor spacing in the denominator. Thus, with similar SDs of the arrival times at the different distances, the larger denominator will result in a smaller fractional error at the longer distances.

The second observation is that the ranking of best to worst location accuracy changes with propagation distance. These changes follow the same pattern that was observed for the dependence of the arrival time errors on propagation distance. The general explanation of this behavior follows exactly the previous explanation given for the ranking in arrival time errors. These factors are the greater "attenuation" of the 522 kHz/S_0 mode as compared to the 60 kHz/A_0 mode with increasing propagation distance; the characteristic of the noise signal having increased noise in the vicinity of the 522 kHz frequency; and the "spreading in time" of the WT magnitudes at low frequencies versus higher frequencies.

Table 7 shows the location errors for the three cases used for the study of the effects of the radiation direction on arrival times at the S/N ratio of 1 to 1. If the order of the best (highest percentage of trials with a location error of 2 % or less) to worst location errors are examined, then the results for cases 9004 and 9030 show little change with the change in radiation angle since the primary frequency/mode combination has a strong dominance at both angles (see Table 7). As before, however, for arrival time errors for case 9002, the rankings of location error accuracy change with the changes in the radiation angle. The change is due to the radiation pattern of the

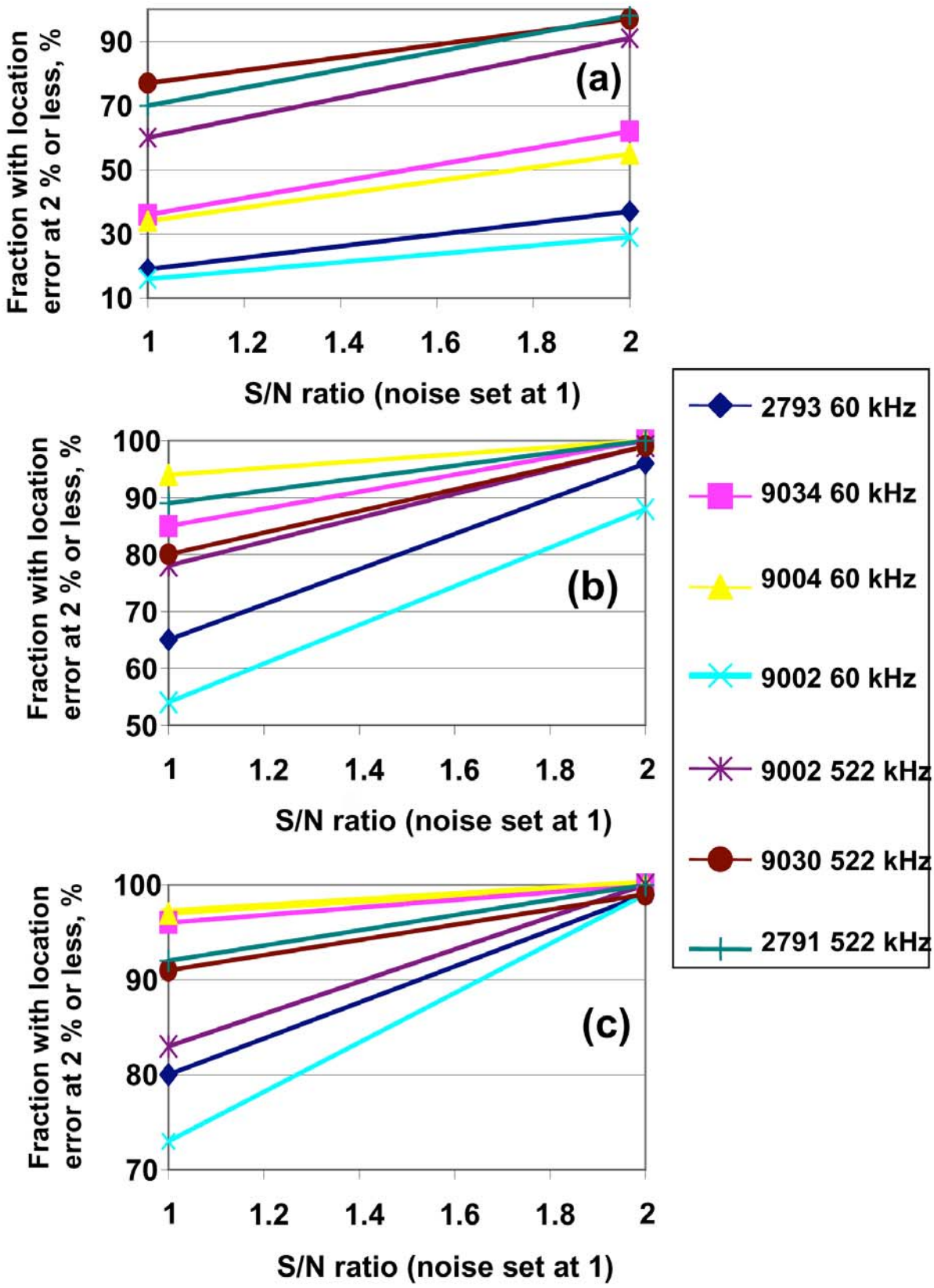

Fig. 11 Fraction of the 1225 calculated locations with an error of 2 % or less at S/N ratios of 1 to 1 and 2 to 1 for all cases (source type and depth) at propagation distances of (a) 60 mm, (b) 120 mm and (c) 180 mm.

two modes not being the same and both modes being significant in the signal. The result is that 9002 (60 kHz/A_0) has a higher fraction with low location error at 45˚, since that mode becomes more dominant at 45˚ versus 0˚. And the opposite is the case for 9002 (522 kHz/S_0), since the effect of the radiation pattern reduces the dominance of that mode at 45˚ versus 0˚.

Table 7 The percentage of the 1225 time differences with a location error ≤ 2 % at two different radiation angles for 180 mm propagation distance and an S/N ratio of 1 to 1.

Case number and (frequency, kHz)	% of trials with location error ≤ 2 % at 0˚.	Ratio: noise-free WT peak at indicated freq./alt. freq. value at zero deg.	% of trials with location error ≤ 2 % at 45˚	Ratio: noise-free WT peak at indicated freq./alt. freq. value at 0˚.	% of trials with location error ≤ 2 % at 67.5˚	Ratio: noise-free WT peak at indicated freq./alt. freq. value at 67.5˚.
9004 (60)	97	4.1	------	--------	97	33
9002 (60)	73	1.01	91	1.5	------	------
9002 (522)	83	0.99	62	0.68	------	------
9030 (522)	91	2.3	------	------	91	3.2

13. Alternate Joint Time-Frequency Analysis Algorithms

Since time-frequency analysis results can be dependent on the particular algorithm used [see reference 11 for a discussion of various techniques], this research also examined the errors in mode arrival times determined when noise is present by the use of alternate (relative to the WT) joint time-frequency analysis algorithms. We choose to use the Adaptive Spectrogram and the Choi-Williams Distribution (spectrogram) in their LabVIEW™ implementations and compared their results with those obtained from the WT. The joint time-frequency analysis (JTFA) algorithms provide the instantaneous power spectrum over time [12]. A number of these JTFA algorithms were available. After using these on some of the FEM-based signals, it was decided to focus on two of them. These were the Easy Adaptive Spectrogram (ADS) and the Easy Choi-Williams Distribution (CWD). The results from either of these can be displayed in a plot of frequency versus time with the colors representing the intensity of the signal energy at the time and frequency values. Figure 12 shows for case 9002 that the JTFA results are qualitatively very similar to the WT results.

In this research both the ADS and CWD results were calculated so as to maintain the 0.1 μs resolution of the original time-domain signals. The frequency resolution could be selected based only on powers of two applied over the range of zero to 5 MHz (based presumably on the Nyquist frequency for the time-domain signals). This led to the choice of a frequency resolution of either 1.22 kHz or 2.44 kHz. To be as consistent as possible with the WT nominal resolution of 3 kHz, the 2.44 kHz resolution was chosen. The ADS results were calculated with the “no-zoom” implementation, the number of terms parameter set at two and the mode parameter selection of “chirplet”. In all other aspects the Easy ADS and CWD implementations were used with the default settings. Also one other selection was made, namely the intensity of the JTFA results was multiplied by 10^{26} to be able to obtain intensity results with larger numbers. These larger numbers were more convenient to use.

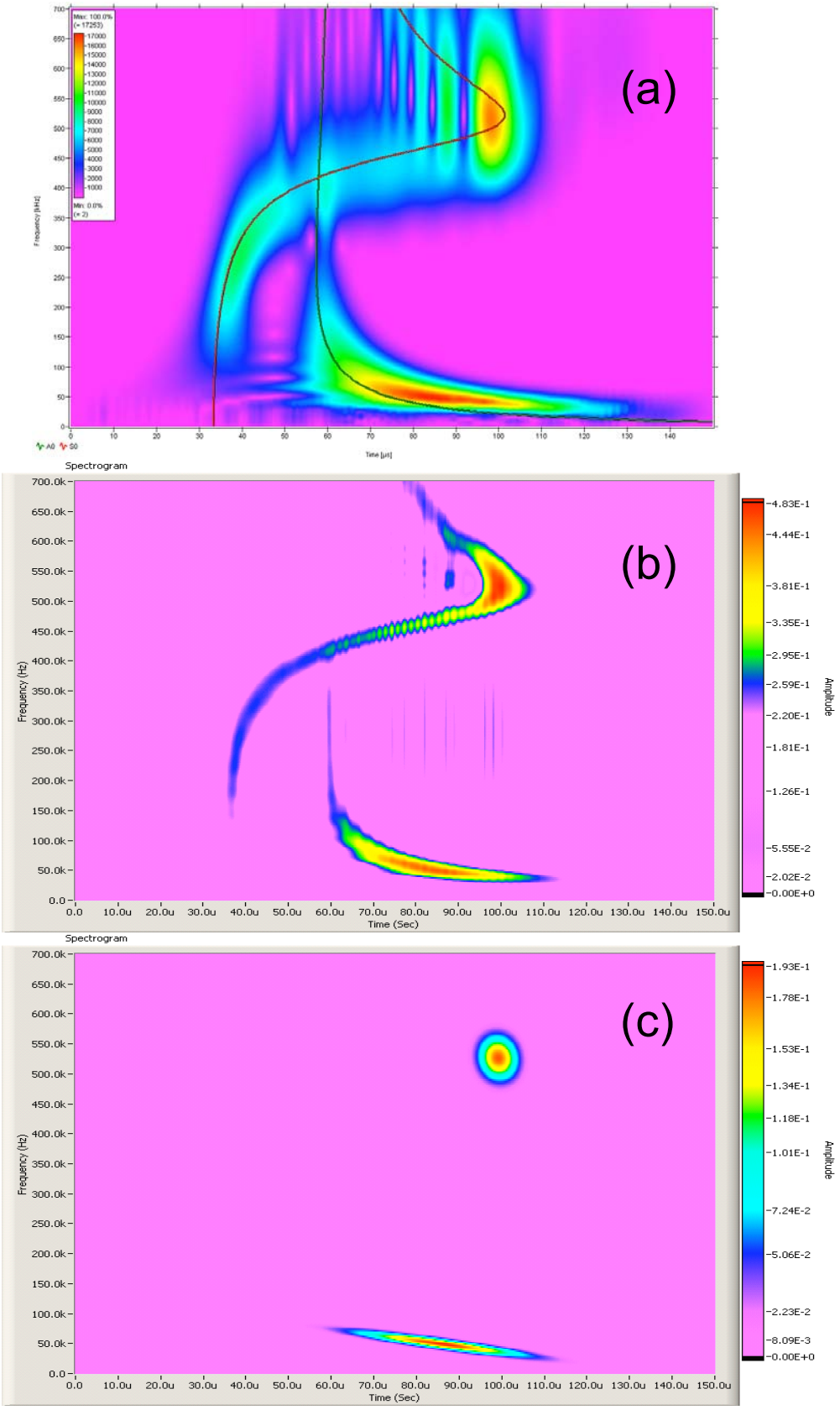

Fig. 12 Spectrograms of WT (a), CWD (b) and ADS (c) for case 9002. Scaling of 0 to 700 kHz vertical and 0 to 150 μs horizontal. Note that non-linear amplitude (color or contrast) scales were used in (b) and (c) to better show the two modes.

14. Comparison of Results with the JTFA and the WT for Noise-free Signals

To create a comparison of the WT with the two selected JTFA spectrograms, the noise-free signals were used for three key cases (9004, 9002 and 9030) in Table 1. The arrival times of the peak magnitudes of the JTFA frequency bands nearest the 60 and 522 kHz values were determined for the dominant frequency/mode in each case for the 0˚ radiation direction and a propagation distance of 180 mm. The nominal frequency bands over which the peak spectrogram magnitudes were determined were (a) WT at 60 to 63 kHz and 522 to 525 kHz and (b) ADS and CWD at 61 to 63.5 kHz and 522.5 to 524.9 kHz. Table 8 shows the results for the noise-free signals compared to the previously determined WT results. As can be seen from the table, the arrival time results are very similar. Thus the peak magnitudes of the key frequencies in the JTFA spectrograms do in fact correspond to the Lamb mode arrivals as was seen for the WT. The table also shows the level of dominance of the primary frequency/mode as determined by the peak magnitude ratios for each case. It is of interest to note that the levels of dominance were generally considerably higher for the CWD and ADS than for the WT.

Table 8 Comparison of noise-free arrival times and relative dominance of the modes for the wavelet transform (WT), Choi-Williams (CWD) distribution and Adaptive (ADS) spectrogram at a propagation distance of 180 mm and direction of 0˚.

Case number and (frequency, kHz) of arrival time	WT noise-free arrival time, µs	Ratio: noise-free WT dominant peak /alt. mode value	CWD noise-free arrival time, µs	Ratio: noise-free CWD dominant peak /alt. mode value	ADS noise-free arrival time, µs	Ratio: noise-free ADS dominant peak /alt. mode value
9004 (60)	78.0	4.1 (60)*	77.3	14 (60)*	75.6	13 (60)*
9002 (60)	78.2	1 (60)*	77.2	1.1 (522)*	75.3	1.3 (522)*
9002 (522)	98.2	1 (60)*	100.0	1.1 (522)*	99.1	1.3 (522)*
9030 (522)	98.0	2.3 (522)*	99.8	6.2 (522)*	99.2	7.8 (522)*

* Most dominant frequency in kHz

15. Comparison of Arrival Time Results with the JTFAs and the WT

To compare the different spectrogram approaches when noise was present, the three cases from the previous section at a propagation distance of 180 mm and the zero-degree propagation direction were used. As before, case 9004 was used since it has a strong dominance of the 60 kHz/A_0 mode. Case 2791 was used since it has a strong dominance of the 522 kHz/S_0 mode. And case 9002 was used since both of the above modes have a significant presence. As was done with the WT, the arrival times were calculated for 50 S+N signals of each of the three cases. Table 9 shows the average arrival times and sample SDs of the peak magnitude determined arrival times for each of the cases at S/N ratios of 1 to 2 and 1 to 1. It should also be recalled that Table 8 shows the level of dominance of the peak mode for each case of the noise-noise signals.

As before, the focus of the relative performance of the different approaches was based on the SDs. Clearly the CWD approach resulted in the lowest SDs followed by the WT and trailed by the ADS. The better performance of the CWD was especially apparent for the S/N ratio of 1 to 2 for cases 9002 and 9030, where the SD with the CWD was substantially lower than that for the

Table 9 Comparison of average arrival times and their SDs (from 50 samples) at S/N ratios of 1 to 2 and 1 to 1 for the Wavelet transform, Choi-Williams distribution and Adaptive spectrogram at a propagation distance of 180 mm and direction of 0˚.

Case number and (frequency*, kHz)	WT 1 to 2, Average and (SD), μs	CWD 1 to 2, Average and (SD), μs	ADS 1 to 2, Average and (SD), μs	WT 1 to 1, Average and (SD), μs	CWD 1 to 1, Average and (SD), μs	ADS 1 to 1, Average and (SD), μs
9004 (60)	77.4 (1.9)	77.4 (1.7)	74.1 (8.1)	77.6 (1)	77.4 (0.72)	74 (6.1)
9002 (60)	78.4 (13)	80.5 (8.8)	60.5 (36)	77.5 (1.9)	77.5 (1.6)	74.9 (20)
9002 (522)	87.7 (28)	92.7 (18.7)	82 (37)	98.1 (4.2)	100 (1.5)	95.5 (13)
9030 (522)	94.2 (15)	100.4 (9)	84.7 (32)	98.1 (1.6)	99.3 (1.4)	99 (1.2)

* Most dominant frequency except for 9002 where both frequencies are significant.

WT. For example, for case 9002 for the 60 kHz/A_0 mode the SD dropped from 13 μs with the WT to 8.8 μs with the CWD, and for the 522 kH/S_0 mode the drop was from 28 μs to 19 μs. The SDs at the 1 to1 S/N ratio were still better with the CWD than with the WT, but the relative improvement was not as large.

16. Conclusions

These direct conclusions are based on the following key conditions: a large 4.7 mm thick aluminum plate; nominal wave propagation distances of 60, 120 and 180 mm; the use of a particular WT; experimental electronic noise from a particular wideband sensor/preamplifier; noise-free signals from finite element modeling that simulates perfect point contact sensors; and the particular six cases of source types and source depths examined in detail.

- Due to the variations in random-noise signals as a function of time, a statistical study of noise-induced errors was necessary.
- At S/N ratios of 1 to 1 and 2 to 1 and a propagation distance of 180 mm in the zero-degree direction, the location error was 2 % or less for at least 73 % and 99 % respectively of the trials considering all six cases.
- At the lower S/N ratios of 1 to 2 and 1 to 1 under the same conditions, the location and arrival time errors were greater if the combination of source type and source depth resulted in a signal with significant energy in portions of both fundamental modes. This result was in contrast to smaller errors in cases where the signal energy was more highly concentrated in a portion of a single mode.
- The order of ranking from smallest to largest errors in location and arrival times changed with propagation distance due to (i) the higher propagation-distance “attenuation” of the 522 kHz/S_0 mode relative to the 60 kHz/A_0 mode, (ii) the higher noise amplitude in the vicinity of 522 kHz, and (iii) the “spreading in time” of the WT magnitude at lower frequencies.
- The order of ranking of errors in arrival times and location also changed with radiation direction changes when the relative WT intensity of the 60 kHz and 522 kHz modes changed with the change of direction.
- Use of the WT technique greatly enhanced the accuracy of arrival times for source location calculations, and also can provide reasonably accurate additional arrival times from AE channels where hits would not even be recorded with threshold based systems. This

- application requires the AE waveform system to record the signals from all the sensors in a local array subset when one sensor channel in that array results in a hit being triggered.
- The errors in location with a fixed threshold are expected to be significantly greater, since the measured arrival times at each hit from a single AE event will correspond to different group velocities due to the factors of geometric attenuation, dispersion, and source amplitude. These factors do not alter the arrival times determined with the WT-based approach.

Alternate Spectrogram Techniques:

The comparison of the WT with the CWD and ADS alternative approaches revealed that the lowest SDs of the arrival times were obtained with the CWD. The improved arrival time results with the CWD were substantial at an S/N ratio of 1 to 2. The poorest results were obtained with the ADS method.

On the Extension of These Techniques to Other Cases

The technique of using the results of joint-time-frequency analysis (such as the WT or CWD) to determine very accurate arrival times (of a certain energetic frequency of a mode corresponding to a specific modal group velocity) in the presence of significant background electronic noise is not expected to be limited to the list of key conditions listed at the beginning of the Conclusion section. The potential main limitation of the approach is possibly for thick plates. In this case, potentially many Lamb modes may be present with significant energy such that either the amplitudes of individual modes making up the time domain are all small and/or the presence of so many energetic modes leads to the extracted mode arrival times not being clearly associated with a particular mode.

References

1. Hamstad, M. A., K. S. Downs and A. O'Gallagher "Practical Aspects of Acoustic Emission Source Location by a Wavelet Transform," Journal of Acoustic Emission, **21**, 2003, 70-94, A1-A7.

2. Hamstad, M. A., A. O'Gallagher and J. Gary, "Examination of the Application of a Wavelet Transform to Acoustic Emission Signals: Part 2. Source Location", Journal of Acoustic Emission, **20**, 2002, 62-81.

3. Gary, John and Marvin Hamstad, "On the Far-field Structure of Waves Generated by a Pencil Break on a Thin Plate," Journal of Acoustic Emission, **12** (3-4), 1994, 157-170.

4. Prosser, W. H., M. A. Hamstad, J. Gary and A. O'Gallagher, "Reflections of AE Waves in Finite Plates: Finite Element Modeling and Experimental Measurements," Journal of Acoustic Emission, **17**, (1-2), 1999, 37-47.

5. Hamstad, M. A., A. O'Gallagher and J. Gary, "Modeling of Buried Acoustic Emission Monopole and Dipole Sources With a Finite Element Technique," Journal of Acoustic Emission, **17** (3-4), 1999, 97-110.

6. Hamstad, M. A., A. O'Gallagher and J. Gary, "Examination of the Application of a Wavelet Transform to Acoustic Emission Signals: Part 1. Source Identification", Journal of Acoustic Emission, **20**, 2002, 39-61.

7. Downs, K. S., Hamstad, M. A., and A. O'Gallagher, "Wavelet Transform Signal Processing to Distinguish Different Acoustic Emission Sources," Journal of Acoustic Emission, **21**, 2003, 52-69.

8. Vallen-Systeme GmbH, Münich, Germany, http://www.vallen.de/wavelet/index.html, 2001, software version R2002.0703.9. Hamstad, M. A., and C. M. Fortunko, "Development of Practical Wideband High Fidelity Acoustic Emission Sensors," Nondestructive Evaluation of Aging Bridges and Highways, Steve Chase, Editor, Proc. SPIE 2456, Published by SPIE – The International Society for Optical Engineering, Bellingham, WA, 1995, pp. 281-288.

10. Hamstad, M. A., "Improved Signal-to-Noise Wideband Acoustic/Ultrasonic Contact Displacement Sensors for Wood and Polymers," Wood and Fiber Science, **29** (3), 1997, 239-248.

11. Huang, Norden E., Zheng Shen, Steven R. Long, Manli C. Wu, Hsing H. Shih, Quanan Zhen, Nai-Chyuan Yen, Chi Chao Tung and Henry H. Liu, "The Empirical Mode Decomposition and the Hilbert Spectrum for Nonlinear and Non-stationary Time Series Analysis." Proc. R. Soc. Lond. A, **454**, 1998, 903-995.

12. LabVIEW™ Signal Processing Toolset, Version 7.0.1, National Instruments Corporation, Austin, TX, 2004.